Electronic Supplementary Material (ESI) for RSC Advances.
This journal is © The Royal Society of Chemistry 2023

Supplementary information for "An Ab Initio DFT Perspective to Experimentally Synthesized $CuBi_2O_4$"

Quazi Shafayat Hossain,[1] Shahran Ahmed,[1] Sadiq Shahriyar Nishat,[2] Md. Zarif Hossain,[1] M. N. I. Khan,[3] Tarique Hasan,[1,4] Muhammad Shahriar Bashar,[5] Mahmuda Hakim,[6] Ishtiaque M. Syed,[7,8,9] Khandker Saadat Hossain,[10] and Imtiaz Ahmed[1,*]

[1] *Materials Science Research Laboratory, Department of Electrical and Electronic Engineering, University of Dhaka, Dhaka-1000, Bangladesh*

[2] *Department of Materials Science and Engineering, Rensselaer Polytechnic Institute, Troy, NY, USA*

[3] *Materials Science Division, Atomic Energy Centre, Dhaka-1000, Bangladesh*

[4] *Department of Physics, University of Jyväskylä, Jyväskylä, 40500, Finland*

[5] *Institute of Fuel Research and Development, Bangladesh Council of Scientific and Industrial Research, Dhaka-1205, Bangladesh*

[6] *Biomedical and Toxicological Research Institute, Bangladesh Council of Scientific and Industrial Research, Dhaka-1205, Bangladesh*

[7] *Department of Physics, University of Dhaka, Dhaka-1000, Bangladesh*

[8] *Semiconductor Technology Research Centre, University of Dhaka, Dhaka-1000, Bangladesh*

[9] *Centre for Advanced Research in Sciences, University of Dhaka, Dhaka-1000, Bangladesh*

[10] *Nanophysics and Soft Matter Laboratory, Department of Physics, University of Dhaka, Dhaka-1000, Bangladesh*

THE DFT CALCULATION PROCEDURE

$$E = F[n]$$

$$= \overbrace{\underbrace{\int d\mathbf{r}\, n(\mathbf{r}) V_{\mathrm{n}}(\mathbf{r})}_{\text{External potential}} - \underbrace{\sum_i \int d\mathbf{r}\, \phi_i^*(\mathbf{r}) \frac{\nabla^2}{2} \phi_i(\mathbf{r})}_{\text{Kinetic energy}} + \underbrace{\frac{1}{2} \iint d\mathbf{r}\, d\mathbf{r}'\, \frac{n(\mathbf{r}) n(\mathbf{r}')}{|\mathbf{r} - \mathbf{r}'|}}_{\text{Hartree energy}} + \underbrace{E_{xc}[n]}_{\text{XC energy}}}^{\text{Total energy in the independent electrons approximation}}. \quad \text{(ES1)}$$

$$\left[-\frac{1}{2}\nabla^2 + V_{\mathrm{tot}}(\mathbf{r}) \right] \phi_i(\mathbf{r}) = \varepsilon_i \phi_i(\mathbf{r}), \quad \text{(ES2)}$$

$$V_{\mathrm{tot}}(\mathbf{r}) = V_{\mathrm{n}}(\mathbf{r}) + V_{\mathrm{H}}(\mathbf{r}) + V_{xc}(\mathbf{r}), \quad \text{(ES3)}$$

$$V_{\mathrm{n}}(\mathbf{r}) = -\sum\nolimits_I \frac{Z_I}{|\mathbf{r} - \mathbf{R}_I|}, \quad \text{(ES4)}$$

$$\nabla^2 V_{\mathrm{H}}(\mathbf{r}) = -4\pi n(\mathbf{r}), \quad \text{(ES5)}$$

$$V_{xc}(\mathbf{r}) = \frac{\delta E_{xc}[n]}{\delta n}(\mathbf{r}), \quad \text{(ES6)}$$

$$n(\mathbf{r}) = \sum\nolimits_i |\phi_i(\mathbf{r})|^2. \quad \text{(ES7)}$$

$$\hat{H}_{\mathrm{n}} = -\sum_I \frac{\nabla_I^2}{2M_I} + U(\mathbf{R}_1, \ldots, \mathbf{R}_M) \quad \text{(ES8)}$$

$$U(\mathbf{R}_1, \ldots, \mathbf{R}_M) = \frac{1}{2} \sum_{I \neq J} \frac{Z_I Z_J}{|\mathbf{R}_I - \mathbf{R}_J|} + E(\mathbf{R}_1, \ldots, \mathbf{R}_M) \quad \text{(ES9)}$$

$$\mathbf{F}_I = Z_I \left[\int d\mathbf{r}\, n(\mathbf{r}) \frac{\mathbf{r} - \mathbf{R}_I}{|\mathbf{r} - \mathbf{R}_I|^3} - \sum_{J \neq I} Z_J \frac{\mathbf{R}_J - \mathbf{R}_I}{|\mathbf{R}_J - \mathbf{R}_I|^3} \right] \quad \text{(ES10)}$$

FIG. S1. DFT Formalism [1]

Setting up the Kohn-Sham Equation

The fundamental assumption of DFT is due to Hohenberg–Kohn where the ground state energy E of the system can be expressed as a functional F of the electron density $n(\mathbf{r})$, i.e., $E = F[n(\mathbf{r})]$[2]. The total energy can be written as Eq. ES1 in Fig. S1 [1]. The terms like external potential, kinetic energy, and Hartree energy in Eq. ES1 can be calculated easily. But the unknown exchange-correlation energy $E_{\mathrm{xc}}[n]$ poses major difficulties in the DFT

simulation. This $E_{\rm xc}[n]$ term can be approximated by different functionals like GGA-PBE, GGA-PBE+U, and HSE06 [3]. The variational principle is used to write the Kohn and Sham equation as Eq. ES2 where ϵ_i and ϕ_i represent single electron eigen energies and eigen functions to be calculated self consistently [4]. The total potential $V_{\rm tot}$ consists of nuclear $V_{\rm n}$, Hartree $V_{\rm H}$ and exchange $V_{\rm xc}$ defined by Eq. ES3-ES7 in Fig. S1. The $\mathbf{R}$ and $\mathbf{r}$ define the nuclear and electronic coordinates respectively.

The Self Consistent Calculation

The self-consistent solution of the Kohn-Sham Eq. ES2 equations provides the total energy of the system under consideration. We summarized the self-consistent calculation in a flow diagram in Fig. S2 [1]. The difficulties arise from the dependence of $V_{\rm H}$ and $V_{\rm xc}$ on the unknown eigenfunction ϕ_i and invoke self-consistency to get around this problem. It is evident the nuclear coordinates $\mathbf{R}_I$s are required for calculating the nuclear potential in V_n. Hence all DFT calculation starts with structural relaxation to find out the nuclear coordinates $\mathbf{R}_I$s.

The Structural Relaxation

For the structural relaxation, the Born-Oppenheimer approximation is used with the nuclear Hamiltonian H_n as shown in Eq. ES8 in Fig. S1. The total nuclear potential energy U are the Coulomb potential among different nuclei with charge Z_I and Z_J following Eq. ES9. The total potential energy U and the density $n(\mathbf{r})$ are used to calculate the Hellman-Feynman force F_I according to the Eq. ES10. From the $\mathbf{F}_I$, the nuclear coordinates are estimated for the relaxed structure in an iterative process as per the flow diagram shown in Fig. S3.

Elastic Properties Calculation

The relevant properties in calculating the elastic properties in DFT are elastic strain ε, stress σ, and elastic tensor C. Both $\varepsilon_{\rm ij}$ and $\sigma_{\rm ij}$ can be expressed as 3×3 matrices with six independent components in each of them [1]. In one index Voigt notation, $\varepsilon_{\rm ij} \rightarrow \varepsilon_{\rm i}$ and $\sigma_{\rm ij} \rightarrow \sigma_{\rm i}$ where $\rm i = 1, 2, 3, 4, 5, 6$ denoting the six independent components. The C relates

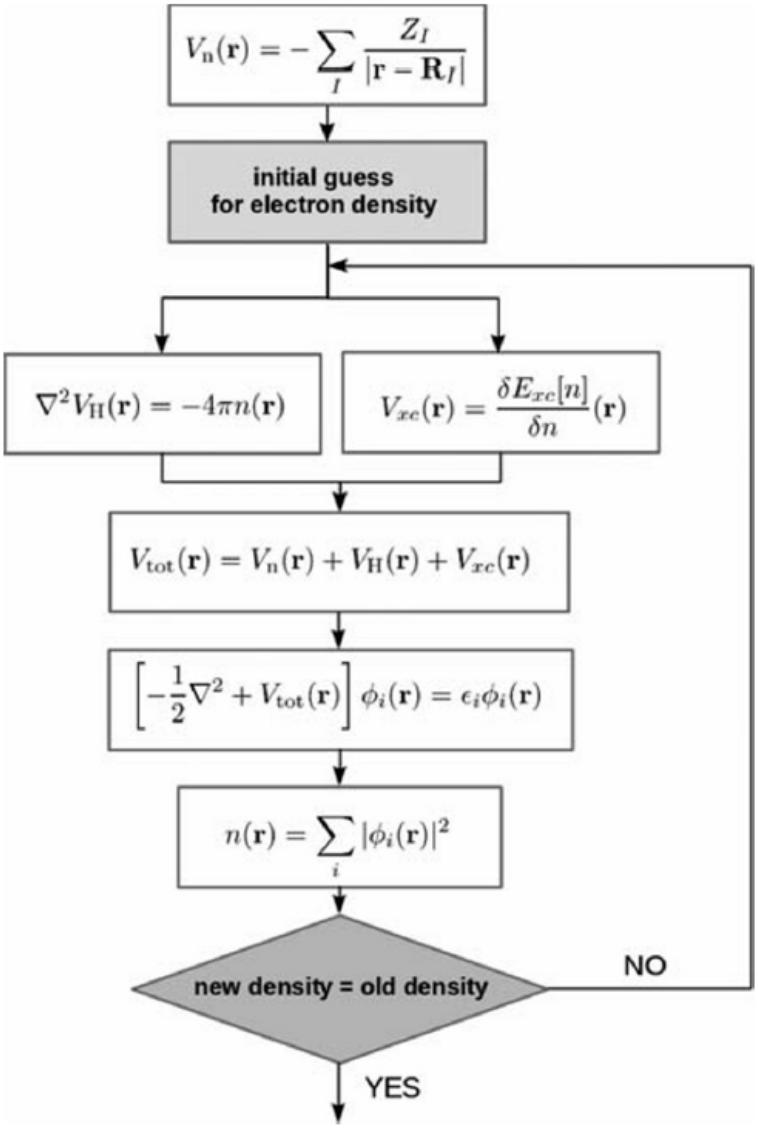

FIG. S2. Flow Diagram of Self-consistent Calculation [1].

the $\varepsilon_{\rm i}$ and $\sigma_{\rm i}$ as $\sigma_{\rm i} = C_{\rm ij}\varepsilon_{\rm j}$. The elastic tensor $C_{\rm ij}$ can be calculated from the estimated self-consistent potential energy ΔU from the relation given by Eq. ES11 below where Ω stands for the unit cell volume.

Electronic Band Structure Calculation

To calculate the electronic band structure (BS), one uses the Eq. ES1 and Eq. ES8 in Fig. S1 to write down the total energy E as shown in Eq. ES12 and Eq. ES13, see

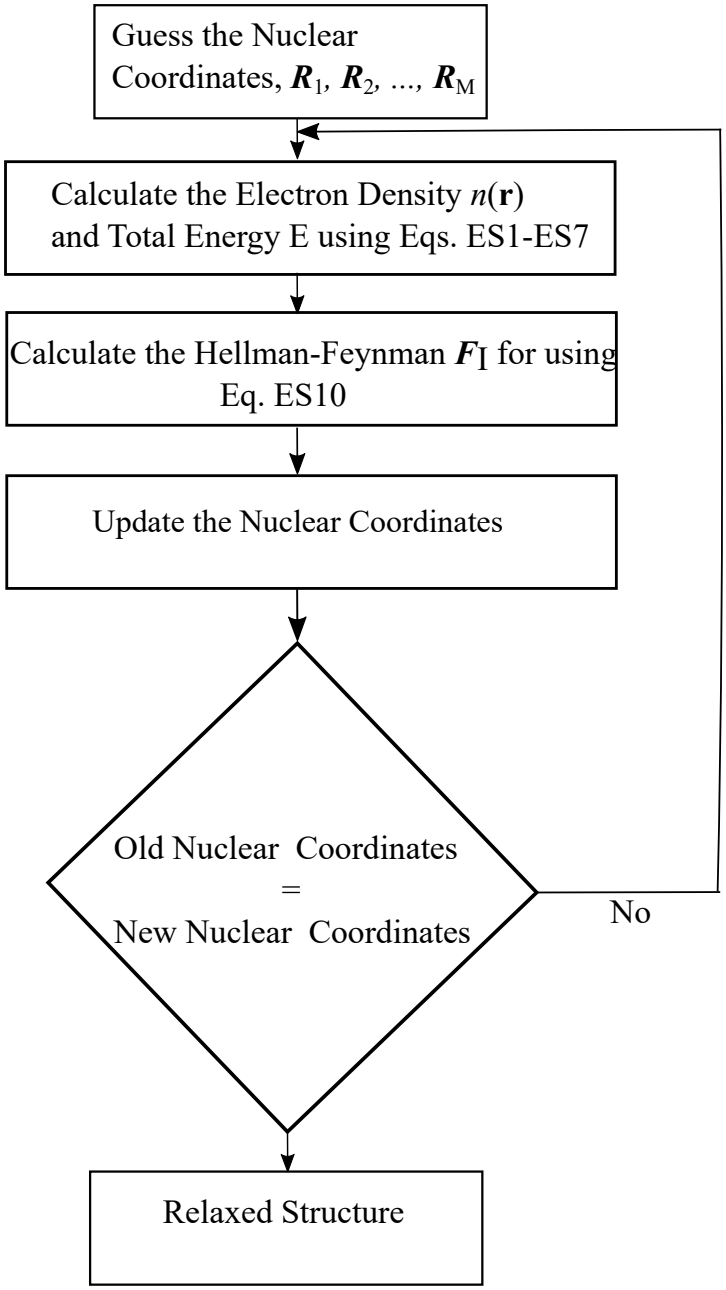

FIG. S3. Flow Diagram of Structural Relaxation in DFT Simulation [1].

$$\frac{\Delta U}{\Omega} = \frac{1}{2} C_{ij} u_i u_j \qquad \text{with} \qquad u_i = \begin{cases} \epsilon_i & \text{if } i = 1, 2, 3 \\ 2\epsilon_i & \text{if } i = 4, 5, 6. \end{cases} \tag{ES11}$$

$$E = \sum_i f_i \int d\mathbf{r}\, \phi_i^*(\mathbf{r}) \left[-\frac{\nabla^2}{2} + V_{\rm n}(\mathbf{r}) + \frac{1}{2} \int d\mathbf{r}' \frac{n(\mathbf{r}')}{|\mathbf{r} - \mathbf{r}'|} \right] \phi_i(\mathbf{r}) + E_{xc}[n] \quad \text{(ES12)}$$

$$E = \sum_i f_i \int d\mathbf{r}\, \phi_i^*(\mathbf{r}) \left[-\frac{\nabla^2}{2} + V_{\rm tot}(\mathbf{r}) \right] \phi_i(\mathbf{r}) - \int d\mathbf{r}\, n(\mathbf{r}) \left[\frac{1}{2} V_{\rm H}(\mathbf{r}) + V_{xc}(\mathbf{r}) \right] + E_{xc}[n] \quad \text{(ES13)}$$

$$\phi_i(\mathbf{r}) \rightarrow \phi_{i\mathbf{k}}(\mathbf{r}) = \mathrm{e}^{i\mathbf{k}\cdot\mathbf{r}} u_{i\mathbf{k}}(\mathbf{r}), \quad \text{(ES14)}$$

where

$$u_{i\mathbf{k}}(\mathbf{r} + \mathbf{T}) = u_{i\mathbf{k}}(\mathbf{r}), \text{ with } \mathbf{T} = n_1\mathbf{a}_1 + n_2\mathbf{a}_2 + n_3\mathbf{a}_3 \quad \text{(ES15)}$$

$$\left[-\frac{1}{2}(\nabla + i\mathbf{k})^2 + V_{\rm tot}(\mathbf{r}) \right] u_{i\mathbf{k}}(\mathbf{r}) = \varepsilon_{i\mathbf{k}} u_{i\mathbf{k}}(\mathbf{r}) \quad \text{(ES16)}$$

$$\hat{H}_{\mathbf{k}}\, u_{i\mathbf{k}} = \varepsilon_{i\mathbf{k}}\, u_{i\mathbf{k}}, \qquad \hat{H}_{\mathbf{k}} = -\frac{1}{2}(\nabla + i\mathbf{k})^2 + V_{\rm tot} \quad \text{(ES17)}$$

$$n(\mathbf{r}) = \sum_i \int_{\rm BZ} \frac{d\mathbf{k}}{\Omega_{\rm BZ}} f_{i\mathbf{k}} |u_{i\mathbf{k}}(\mathbf{r})|^2 \quad \text{(ES18)}$$

$$E = \sum_i \int_{\rm BZ} \frac{d\mathbf{k}}{\Omega_{\rm BZ}} f_{i\mathbf{k}} \varepsilon_{i\mathbf{k}} - \left[E_{\rm H} + \int d\mathbf{r}\, V_{xc}(\mathbf{r}) n(\mathbf{r}) - E_{xc} \right] \quad \text{(ES19)}$$

$$\epsilon_2(\omega) = \frac{\pi\, e^2}{\varepsilon_0 m_e^2 \Omega} \frac{1}{\omega^2} \sum_{cv} \int \frac{d\mathbf{k}}{\Omega_{\rm BZ}} |\langle u_{c,\mathbf{k}} | p_x | u_{v,\mathbf{k}} \rangle|^2 \delta(\varepsilon_{c\mathbf{k}} - \varepsilon_{v\mathbf{k}} - \hbar\omega) \quad \text{(ES20)}$$

FIG. S4. Electronic BS Simulation in DFT [1].

Fig. S4 [1]. In solving the Kohn-Sham equation, the single particle wave functions are written as periodic $u_{i\mathbf{k}}(\mathbf{r})e^{i\mathbf{k}.\mathbf{r}}$ plane wave following Eq. ES14 and Eq. ES15. This plane wave representation converts the single particle Kohn-Sham equation in $\mathbf{k}$ space as shown in Eq. ES16 and Eq. ES17. The electron density $n(\mathbf{r})$ is computed using the planewave representation following Eq. ES18 where $f_{i\mathbf{k}}$ stands for the occupation number of the states. This Brillouin zone (BZ) integral is computed by sampling the BZ using a discrete mesh of wavevectors. Finally in the $\mathbf{k}$ space, the equation for E can be written as shown in Eq. ES19, the solution of which provides the BS i.e. $E - \mathbf{k}$ diagram for material under consideration.

Optical Properties Calculation

The optical properties are revealed through the complex dielectric constant $\varepsilon(\omega) = \varepsilon_1(\omega) + i\varepsilon_2(\omega)$ ($i = \sqrt{-1}$, ω = angular frequency of the optical excitation). Once the BS calculation is done, the $\varepsilon_2(\omega)$ is calculated using a Fermi's golden rule following the Eq. ES20 in Fig.S4 [5]. The standard Kramer-Kronig relations are used to estimate $\varepsilon_1(\omega)$ from $\varepsilon_2(\omega)$ [6]. The optical response is characterized by parameters like absorption coefficient α, reflectivity R, energy loss function L, refractive index η, extinction coefficient K, and optical conductivity σ derived from $\varepsilon(\omega)$ using standard relation [7].

CBO MAGNETIC CONFIGURATIONS

We considered four different spin magnetic configurations, i.e., ferromagnetic (FM), C-type antiferromagnetic (AFM-C), G-type antiferromagnetic (AFM-G), and A-type antiferromagnetic (AFM-A) in the CBO formula unit (f.u.) cell. To probe the spin structure, we fully relaxed the CBO unit cell with 28 atoms by sampling the BZ ($4 \times 4 \times 6$ k points) for both GGA-PBE and GGA-PBE+U functionals using 10^{-8} eV and 10^{-4} eV/Å for electronic and Hellmann–Feynman force convergences respectively. The estimated ground state energies including the non-magnetic (NM) configurations are compiled in Table S1. The 500 eV was used as plane wave energy cutoff.

EDX ANALYSIS

To perform chemical species identification of our samples Energy-dispersive X-ray spectroscopy (EDX) spectra for SCBO and HCBO samples have been obtained as shown in Fig. S5. The weight percent wt. (%) and atomic percent at. (%) of chemical species, Cu, Bi, and O are displayed in Table S2.

Raman Peak Assignment

The room temperature (RT) experimentally observed Raman peaks of SCBO and HCBO samples are benchmarked against that of the DFT simulated ones using LDA, GGA-PBE

CBO Magnetic Configuration Energy									
			Crystal Parameter						
Functional	Mag. Config.	Energy (eV/f.u.)	a (Å)	b (Å)	c (Å)	$\alpha(^\circ)$	$\beta(^\circ)$	$\gamma(^\circ)$	V (Å^3)
GGA-PBE	NM	-154.434	8.491	8.491	6.042	90	90	90	435.611
	FM	-154.779	8.509	8.509	6.046	90	90	90	437.749
	AFM-G	-154.867	8.512	8.512	6.037	90	90	90	437.406
	AFM-A	-154.798	8.519	8.519	6.038	90	90	90	438.198
	AFM-C	-154.869	8.517	8.517	6.033	90	90	90	437.629
GGA-PBE+U	NM	-145.068	8.483	8.483	6.018	90	90	90	433.063
	FM	-147.346	8.499	8.499	6.034	90	90	90	435.854
	AFM-G	-147.368	8.500	8.500	6.032	90	90	90	435.812
	AFM-A	-147.347	8.502	8.502	6.031	90	90	90	435.9445
	AFM-C	-147.369	8.502	8.502	6.030	90	90	90	435.873

TABLE S1. Total energies per CBO formula unit (f.u.) for non-magnetic (NM), ferromagnetic (FM), G-type antiferromagnetic (AFM-G), A-type antiferromagnetic (AFM-A), and C-type antiferromagnetic (AFM-C) of CBO for GGA-PBE and GGA-PBE+U functionals.

EDX Analysis			
Sample	Element	at. (%)	wt. (%)
SCBO	Cu	13.82	10.30
	Bi	32.49	79.62
	O	53.69	10.08
HCBO	Cu	11.18	09.44
	Bi	27.96	77.63
	O	60.86	12.93

TABLE S2. Chemical species identification and atomic percentage at. (%) and weight percentage wt. (%) concentration analysis using EDX of SCBO and HCBO respectively.

and GGA-PBE+U functionals in Table S3. We also marked the relevant symmetry of the underlying lattice vibration and the corresponding atomic motion in CBO.

Fourier Transform Infrared Spectroscopy (FTIR)

The FTIR absorption spectra of SCBO and HCBO were characterized according to the relevant chemical bond vibrations of CBO in Table S4. These RT FTIR peaks were identified

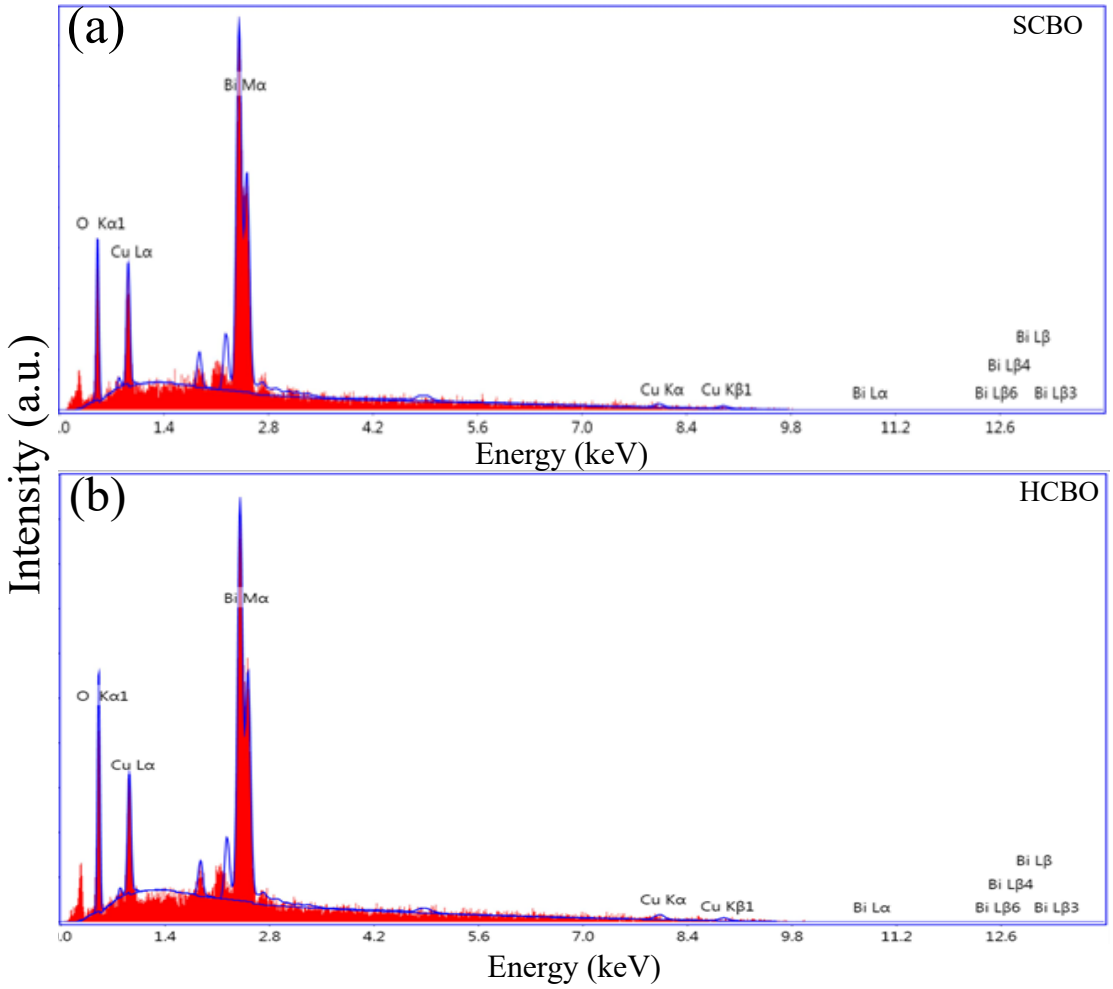

FIG. S5. EDX spectra of (a) SCBO, (b) HCBO

Raman Peak Analysis						
SCBO (cm^{-1})	HCBO (cm^{-1})	LDA (cm^{-1})	GGA-PBE (cm^{-1})	GGA-PBE+U (cm^{-1})	Symm.	Atomic Motion
-	-	44	37	30	A_{1g}	Bi-Bi Motion
85	78	78	85	72	B_{2g}	Bi Rhombohedral Bending
-	128	127	128	128	A_{1g}	CuO_4 Translation
136	-	-	138	138	A_{1g}	CuO_4 Translation
200	191	194	191	194	E_g	Cu-Cu Motion
271	257	260	261	274	A_{1g}	CuO_4 Rotation
300	284	290	308	282	B_{2g}/E_g	CuO_4 Deformation
415	398	398	398	398	A_{1g}	Bi-O Stretching
473	482	480	475	486	B_{2g}	CuO_4 Streching
597	583	585	593	593	A_{1g}/E_g	CuO_4 Breathing
834	830	-	827	825	A_{1g}	CuO_4 Breathing

TABLE S3. Experimental RT Raman peaks of both SCBO and HCBO samples along with that of DFT simulation with LDA, GGA-PBE, and GGA-PBE+U functionals.

FTIR Peak Analysis				
SCBO Exp. (cm^{-1})	HCBO Exp. (cm^{-1})	GGA-PBE (cm^{-1})	GGA-PBE+U (cm^{-1})	Peak Assign.
390	387	377	388	Cu-O
505	544	502	504	Cu-O
672	703	-		Bi-O
830	841	-	-	Bi-O
1052	1040	-	-	Bi-O-Cu
-	1332	-	-	Bi-O
-	1432	-	-	Bi-O

TABLE S4. RT experimental (Exp.) FTIR peaks of both SCBO and HCBO samples are identified from DFPT simulated phonon DOS peaks using GGA-PBE and GGA-PBE+U functionals.

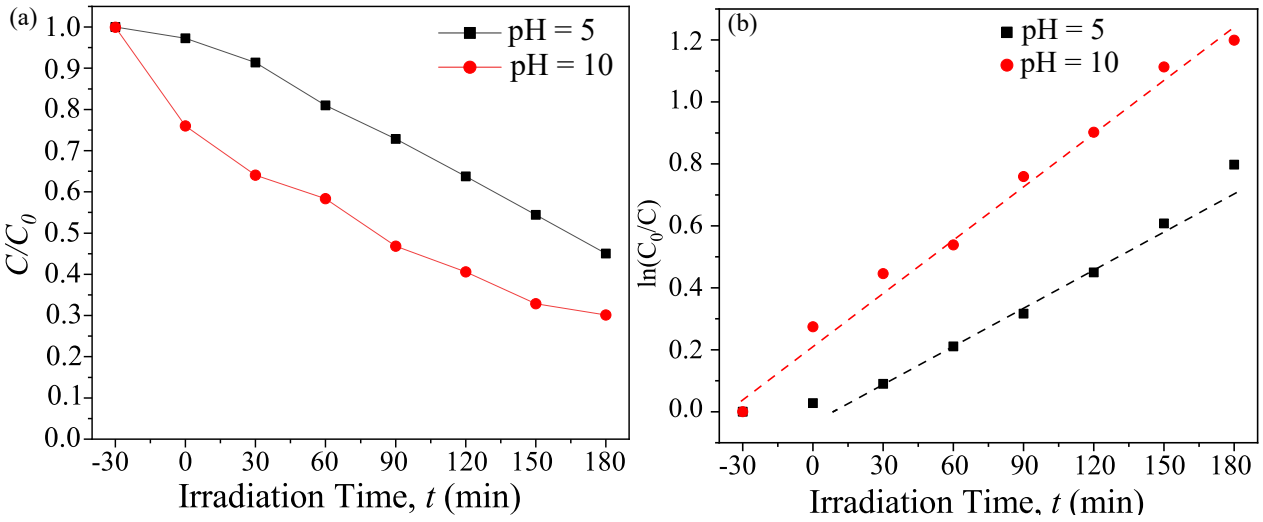

FIG. S6. (a) Time-dependent photocatalytic degradation fraction C/C_0, (b) Linear fitted time-dependent photocatalytic degradation fraction of MB for HCBO (pH= 5, 10).

in the DFPT derived phonon DOS peaks simulated using GGA-PBE and GGA-PBE+U.

PHOTOCATALYTIC MEASUREMENTS

The MB dye degradation fraction C/C_0 is plotted for HCBO sample in cases of pH= 5, 10 as can be seen in Fig. S6(a), where C_0 marks the initial MB dye concentration and C represents the same at some specific irradiation exposure time t. The photocatalytic degradation efficiency (%) of the MB is defined as $(C_0 - C)/C_0 \times 100$. By assuming linear reaction kinematics, the MB dye degradation reaction can be modeled as $\ln(C_0/C) = kt$, where k defines the reaction rate. By linear fitting the $\ln(C_0/C)$ vs. t, as shown in Fig. S6(b), one

can estimate the value of k to be 0.00426 min^{-1} (0.00572 min^{-1}) for the pH of = 5 (10).

---

* imtiaz@du.ac.bd

[1] F. Giustino, *Materials modelling using density functional theory: properties and predictions* (Oxford University Press, 2014).

[2] P. Hohenberg and W. Kohn, Phys. Rev. **136**, B864 (1964).

[3] R. O. Jones, Rev. Mod. Phys. **87**, 897 (2015).

[4] W. Kohn and L. J. Sham, Phy. Rev. **140**, A1133 (1965).

[5] H. Ehrenreich and M. H. Cohen, Phys. Rev. **115**, 786 (1959).

[6] C. Kittel and P. McEuen, *Introduction to solid state physics* (John Wiley & Sons, 2018).

[7] M. Dresselhaus, G. Dresselhaus, S. B. Cronin, and A. G. Souza Filho, *Solid State Properties* (Springer, 2018).